Finite Element Modeling of an AlGaN/GaN Based VOC Sensor Using COMSOL

Balaadithya Uppalapati[1], Akash Kota[2], Vamsy P. Chodavarapu[2], Goutam Koley[1]

[1]Department of Electrical & Computer Engineering, Clemson University, Clemson, SC, USA
[2]Department of Electrical & Computer Engineering, University of Dayton, Dayton, OH, USA
buppala@clemson.edu, kotaa1@udayton.edu, vchodavarapu1@udayton.edu, gkoley@clemson.edu

Abstract

An AlGaN-GaN-AlGaN based dual channel microcantilever has been simulated in COMSOL to compute the temperature profiles in the absence of volatile organic compounds (VOC) at different bias voltages. Simulations are performed by varying the bias voltages from 5 V to 30 V with a step size of 5 V. Using the electric currents (ec) module, the electric field intensity, current density and the electromagnetic loss profiles of the cantilever are obtained. By coupling the ec module with heat transfer (ht) module, the temperature profiles are obtained. From the simulation results, it has been observed that at a bias voltage of 30 V, the cantilever is heated to a highest temperature of $1470\,℃$. Also, at every bias voltage the electric field intensity and temperature is maximum at the tip region of the cantilever.

Keywords: VOC, cantilever, AlGaN, GaN, heat transfer, electric currents.

Introduction

Over the past few years, for monitoring the air quality, detection of volatile organic compounds (VOC) has become extremely important for applications like indoor air quality monitoring, environmental monitoring, health tracking, fire detection, and industrial safety. VOC are a large group of chemicals which can be found in many products that we use to build and maintain our homes. Some of the VOC such as benzene, formaldehyde, ethylene glycol etc. can be found in our everyday life in the form of paints, cleaning agents, and room fresheners. Once these chemicals are in our homes, they are released into the indoor air we breathe. Long term exposure of VOC by human beings will cause adverse health effects. For instance, VOC are the main cause for sick building syndrome [1,2]. Some of the VOC like benzene, and formaldehyde are carcinogenic [3,4]. Therefore, detection of VOC is an essential step in air quality monitoring.

The available technologies to detect the VOC are classified into two categories: nonselective and selective. Sensors such as photoionization and flame ionization detectors are mostly used for nonselective VOC detection. In both sensors, the VOC gas molecules are ionized for detection. But the difference lies in the source of ionization. To ionize the VOC, flame ionization detectors use hydrogen flame, whereas photoionization detectors use high energy (typically 10 eV) ultraviolet photons. The positively charged ions thus generate an electric current which is then amplified by the detector. Even though both sensors exhibit high sensitivity, they lack selectivity [5,6]. To selectively detect the VOC, analytical techniques such as gas chromatography-mass spectrometry (GC-MS) [7,8], and ion mobility-mass spectrometry (IM-MS) [9] are widely used. Selective VOC detection using a typical spectroscopic method involves a two-step process. For instance, in the IM-MS method, first the gas-phase ions are separated based on their size and shape using IM spectrometry. In the second step the separated ions are analyzed by determining their corresponding mass-to-charge ratios using MS. Although these spectroscopic instruments have the advantage of selectivity and high sensitivity, they are bulky and expensive which makes them unfit for portable applications. For in-situ VOC detection, some of the portable sensors such as polymer absorption chemiresistor [10-12], metal oxide sensors [13], and surface acoustic wave sensors [14] are also discussed in the literature. In a Chemiresistor, the electrical resistance is changed due to the chemisorption of VOC molecules. These sensors typically use wheatstone bridge configuration with a chemiresistor in one of the arms. The transducing mechanism of metal oxide sensors is such that when exposed to different VOC, the electrical properties of a metal oxide are changed. In metal oxide sensors resistance or conductivity change is recorded. Materials such as tin oxide (SnO_2) [15], tungsten trioxide (WO_3) [16], zinc oxide (ZnO) [17], and cupric oxide (CuO) [18], are widely used in the development of metal oxide sensors. The response time and range of sensitivities for each of these sensors vary significantly.

Therefore, it is essential to develop a VOC sensor which is portable, sensitive, selective and inexpensive. Micro-electro-mechanical systems (MEMS) based microcantilevers designed using III-nitride semiconductor materials play a significant role in realizing such sensors. In general, III-nitride materials are well known for their applications in high power microwave and power electronic devices owing to their large band gap and unique polarization properties that results in the formation of high sheet charge density and carrier mobility at the heterostructure interfaces [19–22]. III-nitride surfaces have a propensity to interact with polar molecules such as NH_3, NO_2, and ethanol etc., a property that has been exploited to develop gateless III-nitride heterostructure field effect transistors (HFETs). By exposing the gate areas of a HFET with polar molecules, the 2-Dimensinonal Electron Gas (2DEG) is altered at the heterojunction. Using III-nitride materials such as gallium nitride (GaN) and aluminum gallium nitride (AlGaN), single channel and dual channel cantilevers have been demonstrated for VOC detection [23,24].

In this work, a generic finite element model has been developed using COMSOL to simulate the temperature profiles of an AlGaN-GaN-AlGaN based dual channel microcantilever in the absence of VOC at different direct current (DC) bias voltages.

The developed model is useful for validating the experimentally obtained temperature profiles.

Model Geometry

The 3D geometry of the AlGaN-GaN-AlGaN based dual channel cantilever is shown in Fig. 1. The cantilever shown in Fig. 1 comprises 4 layers. From top to bottom, the 4 layers include metal stack 1, metal stack 2, AlGaN and GaN. The thickness of the corresponding metal stacks, AlGaN and GaN layers is 230 nm, 220 nm, 20 nm, and 1.3 µm, respectively. The structure of the cantilever is divided in to three regions namely the base, the intermediate and the tip. The tip region of the cantilever is shown in Fig. 1(b). At the tip region, the gap between the inner and outer AlGaN channels is 3 µm. At the base region, in a typical cantilever the two arms are connected. Instead of simulating the entire cantilever, to reduce the computational load all the support structures are removed. Excluding the base region, the areas of the inner and outer AlGaN channels are 26664 um^2 and 27268 um^2respectively. Similarly, the volumes of the corresponding channels are 266.32 um^3 and 272.32 um^3 respectively. Also, the volume and surface area of the bottom GaN layer is 57833 um^3, and 91352 um^2 respectively.

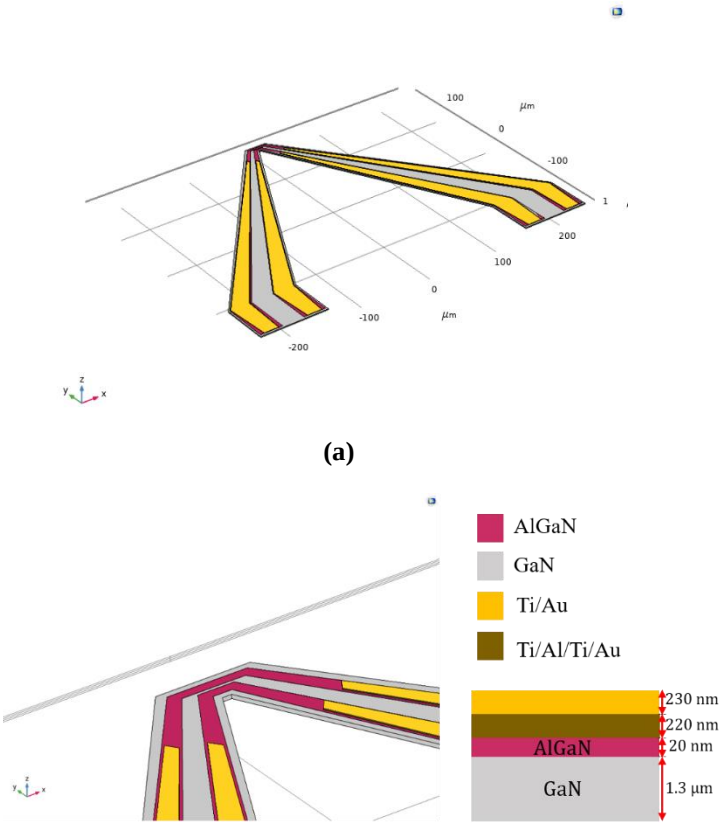

(a)

(b)

Fig. 1. 3D Geometry of the AlGaN-GaN-AlGaN dual channel micro cantilever. **(a)** complete structure, and **(b)** the tip region.

In Fig. 1(b) the metal stack 1 is represented as an alloy Ti/Au made of titanium (Ti) and gold (Au). Similarly, in metal stack 2 there are two alloys Ti/Al and Ti/Au. The Al in metal stack 2 represents aluminum. In a real cantilever, the thickness of an individual metal layer in an alloy is on the order of 50 nm. Instead of representing each metal layer separately, to simplify the problem the alloy stacks are approximated as one layer. The alloy constants are approximated using Vegard's law [25].

Material Properties

To compute the temperature profiles of the cantilever at different bias voltages the required material properties are electrical conductivity (σ), relative permittivity (ϵ_r), thermal conductivity (k), density (ρ) and heat capacity at constant pressure (c_p). Table 1 illustrates the properties of all the materials used in the simulation.

Table 1. List of materials and their respective properties

	GaN	AlGaN	Metal stack 1	Metal stack 2
σ (S/m)	1695	96154	2.6e6	2.6e6
ϵ_r	9.5	8.9	1	1
$k(\text{W}/(\text{m.K}))$	41	52.7	21.9	317
$\rho(\text{kg}/\text{m}^3)$	6150	5740	4506	19300
$c_p(\text{J}/(\text{kg.K}))$	490	490	522	129

Governing Equations

In this model, for the given 3D geometry, the temperature profiles at different bias voltages are computed using the electric currents (ec) and heat transfer (ht) modules in the COMSOL. Using the ec module, electric potential boundary conditions are used to apply the bias voltages on the inner channels. For instance, in this simulation DC bias voltages such as 9 V and 0 V are applied on the edge boundaries of the gold layers located at the left and right arms of the cantilever base region respectively. From the electric potential (V), the equations to compute the profiles of electric field intensity (E), current density (J), and electromagnetic losses (Q_e) on the proposed cantilever structure can be written as

$$E = -\nabla V, \tag{1}$$

$$J = \sigma . E, \tag{2}$$

$$\text{and} \qquad \nabla . J = Q_e. \tag{3}$$

The electromagnetic loss data obtained from the ec module is given as input to the ht module to solve the heat equation which can be written as

$$\left(\rho \cdot c_p \cdot \vec{u}\right) \cdot \nabla T = \nabla \cdot (\vec{q}) + Q_e, \tag{4}$$

$$\text{where} \quad \vec{q} = k \cdot \nabla T. \tag{5}$$

In Eq. (4) $\vec{u}$ is the fluid velocity vector, T is the temperature and $\vec{q}$ is the conductive heat flux. Convective and radiative heat losses are also considered in the simulation. The equation to represent the convective heat loss can be written as

$$-\vec{n} \cdot \vec{q} = q_0, \tag{6}$$

$$\text{where} \quad q_0 = h \cdot (T_{ext} - T). \tag{7}$$

In. Eq. (6) $\vec{q}$ represents the convective heat flux and $\vec{n}$ represents the normal vector pointing in the outward direction. In Eq. (7) q_0 is the inward heat flux, h is the heat transfer coefficient $(\mathrm{W}/(\mathrm{m}^2.\mathrm{K}))$, and T_{ext} is the external environment temperature surrounding the cantilever. For the purpose of simulation, it has been assumed that the cantilever is surrounded by air. Therefore, the values of h and T_{ext} are taken as $5\ \mathrm{W}/(\mathrm{m}^2.\mathrm{K})$ and $293.15\ \mathrm{K}$ respectively. The equation to compute the radiative heat loss can be written as

$$-\vec{n}\cdot\vec{q} = \varepsilon\cdot\sigma\cdot(T_{amb}^4 - T^4), \tag{8}$$

Where $\vec{q}$ represents the radiative heat flux, ε represents the surface emissivity, and T_{amb} represents the ambient temperature of the medium surrounding the cantilever. In this simulation, the values of ε and T_{amb} are taken as 0.9 and 293.15 K respectively.

Simulation Results and Discussion

The simulations are performed to compute the electric field intensity, and temperature profiles of the dual channel cantilever at different bias voltages. The bias voltages are varied from 5 V to 30 V with a step size of 5 V. The simulation results obtained from bias voltages of 10 V, 20 V, and 30 V are shown in Figs. (2), (3) and (4) respectively.

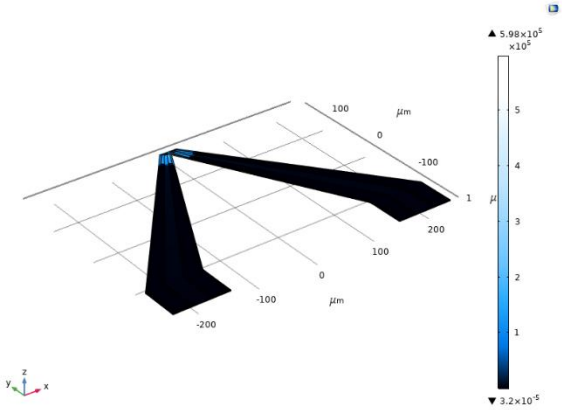

(a)

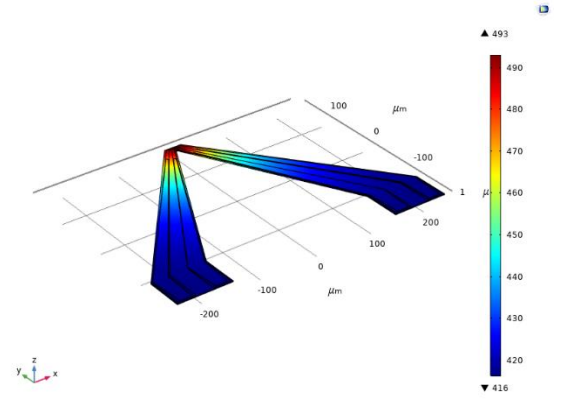

(b)

Fig. 2. Plots of **(a)** Electric field intensity, and **(b)** temperature profile of an AlGaN-GaN-AlGaN dual channel cantilever at a bias voltage of 10 V.

From Fig. 2 the electric field intensity and temperature is maximum at the tip region of the cantilever. The corresponding magnitudes are $5.98\times10^5\ \mathrm{V/m}$ and 493 ℃ respectively.

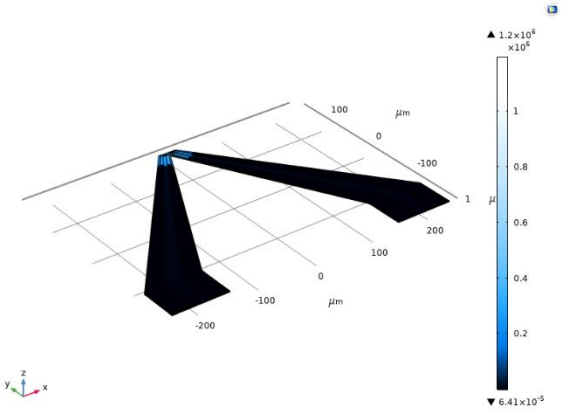

(a)

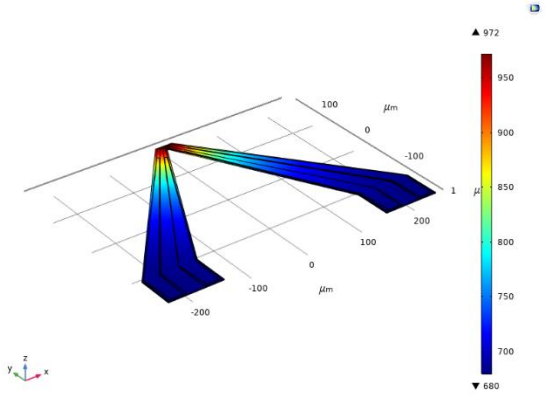

(b)

Fig. 3. Plots of **(a)** Electric field intensity, and **(b)** temperature profile of an AlGaN-GaN-AlGaN dual channel cantilever at a bias voltage of 20 V.

In Fig. 3, when the bias voltage is increased from 10 V to 20 V, at the tip region the magnitude of electric field intensity has been increased from $5.98\times10^5\ \mathrm{V/m}$ to $1.2\times10^6\ \mathrm{V/m}$. Similarly, the magnitude of temperature has also been increased from 493 ℃ to 972 ℃.

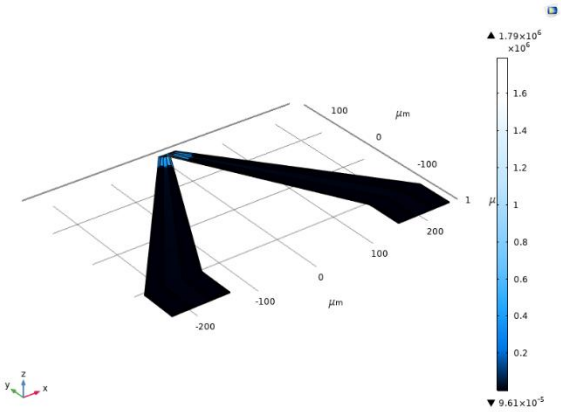

(a)

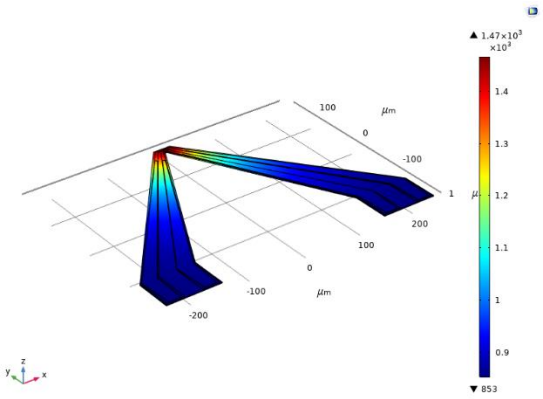

(b)

Fig. 4. Plots of **(a)** Electric field intensity, and **(b)** temperature profile of an AlGaN-GaN-AlGaN dual channel cantilever at a bias voltage of 30 V.

In Fig. 4, when the bias voltage is increased from 20 V to 30 V, at the tip region the magnitude of electric field intensity has been increased from 1.2×10^6 V/m to 1.79×10^6 V/m. Similarly, the magnitude of temperature has also been increased from 972 ℃ to 1470 ℃.

Conclusions

An AlGaN-GaN-AlGaN based dual channel cantilever has been simulated in COMSOL to obtain the temperature profiles at different DC bias voltages. To perform the simulations the electric currents and heat transfer modules are coupled. The DC bias voltages are varied from 5 V to 30 V with a step size of 5 V. From the simulation results, it can be concluded that at every bias voltage the magnitude of electric field intensity and temperature is maximum at the tip region of the cantilever. Also, as the applied bias voltage increases, the electric field intensity and temperature also increases. At a bias voltage of 30 V, the cantilever is heated to the highest temperature of 1470 ℃. The numerical results obtained from these simulations are useful for validating the experimental results. The temperature profiles of a cantilever can be experimentally obtained using a thermal imaging camera.

References

1. J.T. Brinke *et.al*, "Development of new volatile organic compound (VOC) exposure metrics and their relationship to sick building syndrome symptoms," *Indoor Air*, **8**, 140–152 (1998).
2. P.S. Burge, "Sick building syndrome," *Occup. Environ. Med.*, **61**, 185–190 (2004).
3. World Health Organization, "WHO Guidelines for Indoor Air Quality: Selected Pollutants," Geneva (2010). Available online:http://www.euro.who.int/__data/assets/pdf_file/0009/128169/e94535.pdf.
4. H. Guo, S.C. Lee, L.Y. Chan, and W.M. Li, "Risk assessment of exposure to volatile organic compounds in different indoor environments," *Environ. Res.*, **94**, 57–66 (2004).
5. Y. Zhou *et.al*, "Application of portable gas chromatography-photo ionization detector combined with headspace sampling for field analysis of benzene, toluene, ethylbenzene, and xylene in soils," *Environ. Monit. and Assess.*, **185**, 3037–3048 (2013).
6. L. Spinelle *et al.*, "Review of Portable and Low-Cost Sensors for the Ambient Air Monitoring of Benzene and Other Volatile Organic Compounds," *Sensors*, **17**, 1520 (2017).
7. J.S. Kim, H.W. Yoo, H.O. Choi, and H.T. Jung, "Tunable volatile organic compounds sensor by using thiolated ligand conjugation on MoS2," *Nano Lett.*, **14**, 5941–5947 (2014).
8. B. Buszewski *et al.*, "Analysis of exhaled breath from smokers, passive smokers and nonsmokers by solid phase microextraction gas chromatography/mass spectrometry," *Biomed. Chromatogr*., **23**, 551–556 (2009).
9. A. B. Kanu *et al.*, "Ion mobility–mass spectrometry," *Int. J. Mass Spectrom.* , **43**, 1-22 (2008).
10. C.D Natale *et al.*, "Lung cancer identification by the analysis of breath by means of an array of non-selective gas sensors," *Biosens. Bioelectron*., **18** 1209–1218 (2003).
11. I. Elmi *et al.*,"Development of ultra-low-power consumption MOX sensors with ppb-level VOC detection capabilities for emerging applications," *Sens. Actuators B Chem.*, **135**, 342-351 (2008).
12. N. Tang, Y. Jiang, H. Qu, and X. Duan "Conductive polymer nanowire gas sensor fabricated by nanoscale soft lithography," *Nanotechnology.*, **28**, 485301 (2017).
13. N. Tang *et al.*, "A fully integrated wireless flexible ammonia sensor fabricated by soft nano-lithography," *ACS Sensors*., **4**, 726–732 (2019).
14. J.W. Grate *et al.*, "Smart sensor system for trace organophosphorus and organosulfur vapor detection employing a temperature-controlled array of surface acoustic wave sensors, automated sample preconcentration, and pattern recognition," *Analytical Chemistry*, **65**, 1868–1881 (1993).
15. J. Getino, J *et al.*, "Analysis of VOCs with a tin oxide sensor array," *Sens. Actuators B Chem.*, **43**, 200–205 (1997).
16. W. Zhang *et al.*, "Ultrafine Tungsten Oxide Nanowires: Synthesis and Highly Selective Acetone Sensing and Mechanism Analysis," *ACS Appl. Mater. Interfaces*, **12**, 3755-3763 (2019).
17. S.G. Leonardi, "Two-dimensional zinc oxide nanostructures for gas sensor applications," *Chemosensors*, **5**, 17 (2017).
18. O.Lupan *et al.*, "Single and networked CuO nanowires for highly sensitive p-type semiconductor gas sensor applications," *physica status solidi (RRL)–Rapid Research Letters*, **10**, 260–266 (2016).
19. T.J. Flack, B.N. Pushpakaran, and S.B. Bayne, "GaN Technology for Power Electronic Applications: A Review," *J. Electron. Mat.* , **45**, 2673–2682 (2016).
20. G. Simin *et al.*, "III-nitride microwave control devices and ICs," *Semiconductor Science and Technology*, **28**, 74008 (2013).
21. M. Stutzmann *et al.*, "GaN-based heterostructures for sensor applications," *Diamond and Related Materials*, **11**, 886–991 (2002).
22. M. Rais-Zadeh *et al.*, "Gallium Nitride as an Electromechanical material," *J. Microelectomech. Syst.*, **23**, 1252–1271 (2014).
23. I. Jahangir, E.B. Quddus, and G. Koley, "Unique detection of organic vapors below their auto-ignition temperature using III–V Nitride based triangular microcantilever heater," *Sens. Actuators B Chem.*, **222**, 459-467 (2016).

24. S. Gorman, D. Gajula, S. Kim and G. Koley, “Impact of volatile organic compound exposure on electrical breakdown in GaN dual channel microcantilevers,” *Appl. Phys. Lett.*, **114**, 114103, (2019).
25. N. DeRoller, M. Qazi, J. Liu, and G .Koley, “Characterization of an AlGaN/GaN electrostatically actuated cantilever using Finite Element Method,” in *Proc. COMSOL conf.*, Boston (2010).